Maria KOTELKO
Martin MACDONALD
Muditha P. KULATUNGA
Zuzanna MARSZALEK

UPPER-BOUND ESTIMATION OF LOAD-CARRYING CAPACITY OF PERFORATED COLD-FORMED THIN-WALLED STEEL LIPPED CHANNEL COLUMNS UNDER COMPRESSION LOADING

OSZACOWANIE GÓRNE NOŚNOŚCI PERFOROWANYCH ZIMNO FORMOWANYCH PRĘTÓW CIENKOŚCIENNYCH PODDANYCH ŚCISKANIU

Upper-bound estimation of the load-capacity of cold-formed steel sections (TWCFS) with perforations, subjected to axial compression is presented. The estimation is performed on the basis of the Yield Line Analysis ((YLA). TWCFS lipped channel sections with two sets of perforations (on the web and on the flanges) are under investigation. The comparison of experimental results, FE simulation results, European code ultimate strength predictions and upper-bound estimation based on YLA approach is carried out and presented. Some conclusions concerning an applicability of the YLA approach for ultimate strength prediction of perforated TWCFS structural members are derived.

Keywords: cold-formed steel, thin-walled structures, load-capacity, perforations.

W artykule przedstawiono wyniki górnego oszacowania nośności cienkościennych prętów zimno formowanych z perforacjami, poddanych osiowemu ściskaniu. Oszacowanie to jest oparte na metodzie załomów plastycznych. Rozpatrywano dwa warianty perforacji (środnika i pasów) cienkościennych prętów ceowych z żebrami końcowymi. Przeprowadzono analizę porównawczą wyników eksperymentu, wyników symulacji numerycznych MES oraz wyników obliczeń wg wzorów normatywnych normy europejskiej z wynikami oszacowania górnego nośności opartego na metodzie załomów plastycznych. Sformułowano wnioski dotyczące możliwości zastosowania tej metody do szacowania nośności cienkościennych prętów zimno formowanych z perforacjami.

Słowa kluczowe: stal zimno formowana, konstrukcje cienkościenne, nośność, perforacje.

1. Introduction

Nowadays, a variety of different steel products, with a large diversity of shapes, sizes, and applications are produced using the cold-forming process. The range of use of TWCFS is very wide, including buildings, the automobile industry, shipbuilding, rail transport, the aircraft industry, highway engineering, agricultural and industry equipment, office equipment, chemical, mining, petroleum, nuclear and space industries. Compared to their hot-rolled counterparts, thin-walled cold-formed steel structural members can provide more economical and efficient design solutions due to several advantages, such as a light weight, a high flexibility in obtaining various cross-sectional shapes, a highly adaptable manufacturing process with relatively little waste, and easier and faster construction. Perforations are used in many TWCFS members to accommodate services such as electrical, plumbing, and heating. They are particularly used in storage racks and in low- to mid-rise multi-storey buildings and portal frames.

Because of the thinness of section walls and the wide variety of shapes which can be used (stiffeners, lips, etc.), some specific types of buckling, which are not observed in other thin-walled structures, can appear in cold-formed steel profiles. Particularly, symmetric and anti-symmetric buckling modes, for which buckling loads are of very close values [33] as well as coupled buckling modes [4].

Thus, stability and load carrying capacity problems, related to those members, induce particular aspects which are new challenges for researchers who work on new theoretical solutions (both analytical and numerical) and it has stimulated a development in the Theory of Stability and Theory of Thin-Walled Structures, especially in recent years. The problem of the load carrying capacity of such members subjected to simple loading systems (pure bending or uniform compression) has been with satisfactory accuracy solved within the theory of thin-walled structures, as well as in design code specifications [29, 31, 39]. This theory provides sufficient methods of the load-carrying capacity evaluation, among them effective width method [12, 39], Direct Strength Method – DSM [24, 30]. Such a method should well satisfy the target reliability index in structural design [37]. Very recently, structural analyses and reliability studies that implement the system-based design-by-analysis of steel thin-walled structure (rack frames) has been presented by Cardoso et al [3]. The analysis was based on Direct Design Method (DDM), modification of DSM method.

However, there are relatively few reports of research, that have been carried out in the analysis of TWCFS members with perforations subjected to compression loading. The state of art review indicates, that the buckling and ultimate strength of such a structure under compression depends strongly on the shape, size and location of perforations [21]. Davies et al [5] proposed an analytical method of design of axially compressed perforated steel sections, based on the effective

thickness approach. Kulatunga et al published results of theoretical and experimental analysis of cold-formed steel members under compression [17, 19, 20]. Moen and Schafer applied the Direct Strength Method (DSM) to the analysis of cold-formed steel columns with holes [23] and compared the results with results of experiments [25]. Inelastic buckling of perorated plates and sections under compression with perforations was investigated by Yao and Rasmussen [38]. The problem of the structural behaviour of plates with special type of perforations (cut-outs) in inelastic range was analysed, using Finite Element Method, by Falkowicz [6]. Buckling load of non-standard thin-walled channel beams with perforations, subject to bending, was investigated by Grenda [8] and Magnucka-Blandzi [23]. Also, Nedelcu [28] analysed buckling mode decomposition of thin-walled members with holes. However, the above state -of -art review shows, that reliable design specifications to predict the ultimate buckling strength of perforated steel sections are not yet available. Thus, research into an effective method to evaluate load-carrying capacity of those structures (closely related to the structure's reliability assessment) is still an open question (particularly for members undergoing local buckling). Analytical or semi-analytical methods, based on effective thickness approach, for relatively short perforated members have been not reported so far. As mentioned above, Davies [5] proposed such a method, but it was applicable for relatively long members, for which global buckling takes place.

In this paper results of numerical (finite element FE), experimental and theoretical investigations based on the Yield Line Analysis (YLA) approach associated with effective thickness approach are presented, and conclusions are drawn on this basis. The conclusions are mainly focused on the applicability of the YLA approach to the upper-bound estimate of load-carrying capacity of TWCFS members with perforations. Preliminary, selected results of the YLA analysis are presented in [22]. This approach is competitive in comparison with FE analysis or other numerical and analytical-numerical methods, since algorithms based on it are simple and calculation time is very short, in comparison with very time-consuming FE calculations. The state of art review presented above indicates, that the YLA approach has not been applied to evaluate ultimate strength of perforated thin-walled members so far.

A thin- walled structure is characterized by a certain "redundancy" of its load-carrying capacity (l-c-c). In order to evaluate this "redundancy, one has to solve the problem of stability and post-buckling behaviour of the structure, as well as the problem of failure (post-ultimate) behaviour, i.e. to estimate the upper-bound load-carrying capacity. That estimation consists in the determination of the intersection–point of a post-buckling path (evaluated using either analytical, semi-analytical method or a numerical method, e.g. Finite Element Analysis) and a rigid-plastic *post-ultimate curve* obtained from the Yield Line Analysis (YLA) [14].

Short thin-walled columns (classified in European design code as members of class 4) subjected to compression and/or bending undergo local or distortional buckling. The failure of such members is initialised by the local-global interactive buckling of plastic-elastic type, not an elastic-elastic one. Thus, the failure of those members, either in compression or bending, is always initialized by the development of a local plastic mechanism in one of the member's walls. The problem of the load carrying capacity (l-c-c) of such members subjected to simple loading systems (pure bending or uniform compression) has been satisfactorily solved within the theory of thin-walled structures, as well as in design code specifications [32]. However, the same problem for members of non-standardised sections or shapes, and, particularly with perforations, is still an open question and worthy of further investigation. One of the solutions is an appropriate upper-bound estimation of l-c-c.

2. Subject of the analysis

The subjects of the analysis were lipped channel cross-section columns with perforations located either on the web or flanges (Figures 1 and 2). Tables 1-5 illustrate the columns dimensions, location and dimensions of perforations and material parameters taken into account in this research. The presented research is a continuation of research, the results of which (mainly experimental) have been partially published by Macdonald [22]. All investigated columns were of the same length and the same cross-section dimensions. In both sets the position of perforations (distance from the ends) was constant, but with different perforation areas (perforation diameters).

3. Numerical FE analysis

To study the structural behaviour (buckling, post-buckling and ultimate) of examined sections, the non-linear analysis was applied, using ANSYS numerical code. Detailed description of FE numerical model (geometry, boundary conditions), are given in [22]. ANSYS element type SHELL181 was used as it is adequate for linear, large rotation, and/or large strain nonlinear applications. Load was applied through a load bearing plate which represents the actual loading conditions applied in the experiments. ANSYS element type SOLID45 was used to model the load bearing plates [1] [9] [18]. Fine mesh around

Table 1. Column dimensions and material properties.
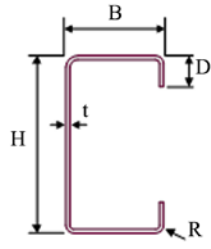
	Cross-section dimensions	
	H (mm)	120.00
	B (mm)	50.00
	D (mm)	15.00
	R (mm)	3.00
	t (mm)	1.15
Average yield strength, sy (N/mm2)		195
Modulus of elasticity, E (N/mm2)		210500
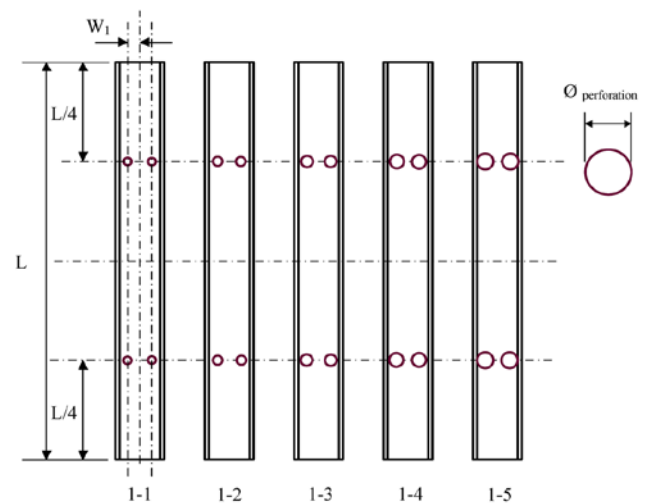
Fig. 1. Shape and location of perforations – Set 1 - perforations located on the web, [22]

Table 2. Nominal dimensions of perforations – Set 1

Column	Length of the column	Ø perforation	W1
1-1	L	3 b	c
1-2	L	4 b	c
1-3	L	5 b	c
1-4	L	6 b	c
1-5	L	7 b	c
		L = 1000 mm, b = 5 mm, c = 30 mm	
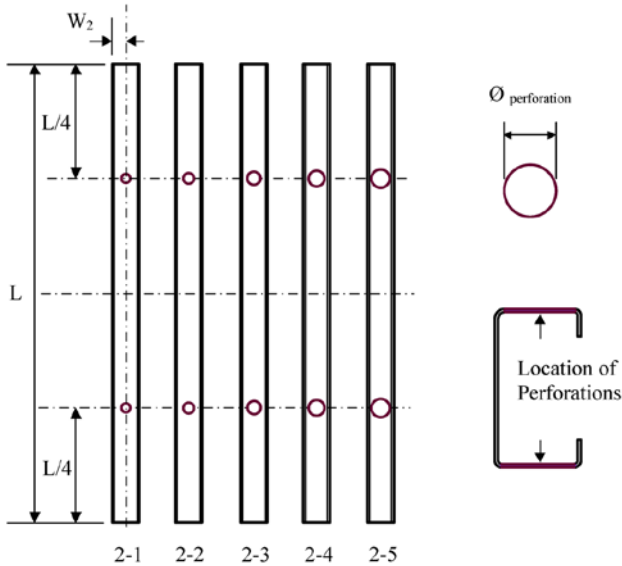
Fig. 2. Shapes and location of perforations - perforations located on the flanges – Set 2 [22]

Table 3. Nominal dimensions of perforations – Set 2

Column	Length of the column	Ø perforation	W2
2-1	L	3 b	c
2-2	L	4 b	c
2-3	L	5 b	c
2-4	L	6 b	c
2-5	L	7 b	c
		L = 1000 mm, b = 5 mm, c = 25mm	

Table 5. Actual measured dimensions and location of perforations

	Column Ref.	Ø perforation (mm)	Perforation position measured from bottom end (mm)
Set 1	1-1	15.02	250.02
		15.04	250.06
		15.00	750.00
		15.06	750.08
	1-2	20.80	250.04
		20.22	250.00
		20.00	750.04
		20.72	750.02
	1-3	25.02	250.00
		25.06	250.02
		25.00	750.06
		25.04	750.04
	1-4	30.02	250.02
		30.04	250.00
		30.00	750.06
		30.02	750.04
	1-5	35.04	250.02
		35.02	250.04
		35.00	250.02
		35.02	250.06
Set 2	2-1	15.02	250.02
		15.00	250.00
		15.04	750.04
		15.06	750.06
	2-2	19.98	250.02
		20.00	250.00
		20.02	750.06
		20.04	750.02
	2-3	25.00	250.02
		24.98	250.06
		25.02	250.00
		25.00	250.02
	2-4	30.02	250.02
		30.04	250.00
		30.02	250.04
		30.06	250.06
	2-5	35.02	250.02
		35.00	250.00
		35.04	750.04
		34.98	750.04

Table 4. Actual measured section dimensions

	Column Ref.	Web height, H (mm)	Flange length, B (mm)	Lip height, D (mm)	Corner radius, R (mm)	Thickness, t (mm)	Total length, L(mm)
Set 1	1-1	120.20	50.10	15.12	3.00	1.15	1000.20
	1-2	120.00	49.20	14.20	3.00	1.15	1000.00
	1-3	120.10	49.52	14.92	3.00	1.15	1000.40
	1-4	120.42	51.54	14.90	3.00	1.15	1000.10
	1-5	120.62	50.80	15.62	3.00	1.15	1000.20
Set 2	2-1	120.12	49.86	14.90	3.00	1.15	1000.30
	2-2	120.24	50.12	15.32	3.00	1.15	1000.30
	2-3	120.16	50.02	15.08	3.00	1.15	1000.30
	2-4	121.22	50.80	15.92	3.00	1.15	1000.40
	2-5	120.62	50.82	15.84	3.00	1.15	999.90

Fig. 3. Tinius olsen structural testing machine and column specimen set-up
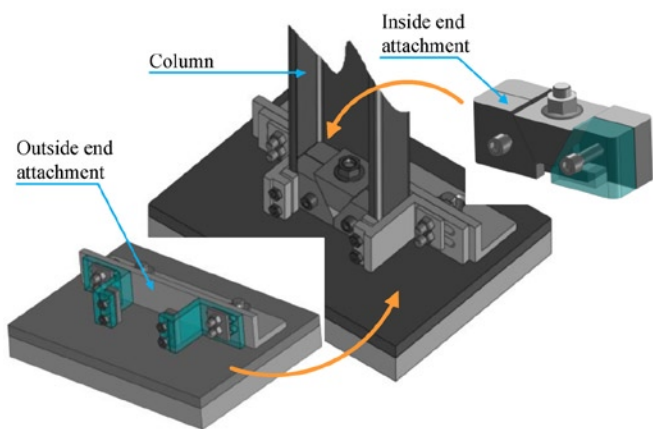
Fig. 4. Clamping grips, keeping a column specimen in a built-in position [22]
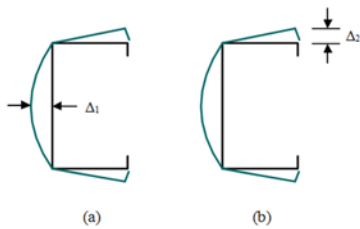
Fig. 5. Definition of geometric imperfections, (a) Type 1: geometric imperfections can be seen in a stiffened element and (b) Type 2: maximum deviation from straightness for a stiffened lip or un-stiffened flange [31]

perforations and coarse mesh further away from the perforations was applied [22]. Fixed-fixed (built-in) boundary condition where applied in FE model, adequate to actual experiments conditions.

4. Experimental Investigation

4.1. Experimental stand and specimens

All columns, with dimensions and all other testing parameters specified in Tables 1-5 were tested in the whole range of loading up to and beyond the ultimate load - to failure. All tests were carried out on the columns with fixed-fixed (built -in) boundary conditions. Experimental results reported in the next paragraphs, were used to validate Finite Element analysis results and upper-bound estimation results of the columns load-carrying capacity, based on YLA analysis. The tests were performed on the Tinius-Olsen testing machine. All column specimens were loaded with displacement control at a constant rate. A linear displacement transducer (LVDT) of high accuracy was used to measure the Tinius-Olsen testing machine crosshead displacement as shown in Figure 3.
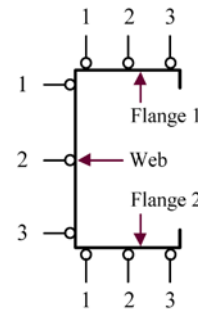
Fig. 6(a). Locations on the web and flanges to measure geometric imperfections.

Due to their comparative thinness, cold-formed thin-walled steel sections can deform easily during handling and hence, these sections can have higher initial geometric imperfections. Due to the nature of the geometric imperfections, they are categorised into two types namely, Type 1 and Type 2 as illustrated in Figure 5.

Figure 5: Definition of geometric imperfections, (a) Type 1: geometric imperfections can be seen in a stiffened element and (b) Type 2: maximum deviation from straightness for a stiffened lip or un-stiffened flange [31].

In this investigation, measurements were documented along three lines in the longitudinal direction in both web and flanges at 20 mm intervals using a co-ordinate measuring machine to a precision of 0.01 mm as presented in Figure 6. The exact values of measured dimensions are given in Tables 4 and 5.

A set of experiments was carried out to study the influence of a perforation area on the buckling and ultimate strength of column members. As mentioned above, the specimens were selected to have same cross-section dimensions, but with different perforation (Figures 2,3). The column lengths were kept constant.

4.2. Structural behaviour of tested columns

All tested columns behaved in a very similar way in whole range of loading, up to the ultimate load and beyond – in the post-ultimate stage. Buckling occurred in all specimens around 85% of the ultimate load, which corresponded to the buckling load obtained in FE calculations. All the specimens failed by local buckling, interacting with distortional buckling, at the peak load forming three local-distortional buckling half-waves. Maximum deformation occurred around the perforations near to the bottom end in the specimens set 1-2 to set 1-4 whereas, in specimens 1-1 and 1-5, the maximum deformation occurred around the perforations near to the top end. In all tested specimens the failure was initiated in the area of perforation and, subsequently, local plastic mechanisms were developed in this area (see Figure 7).
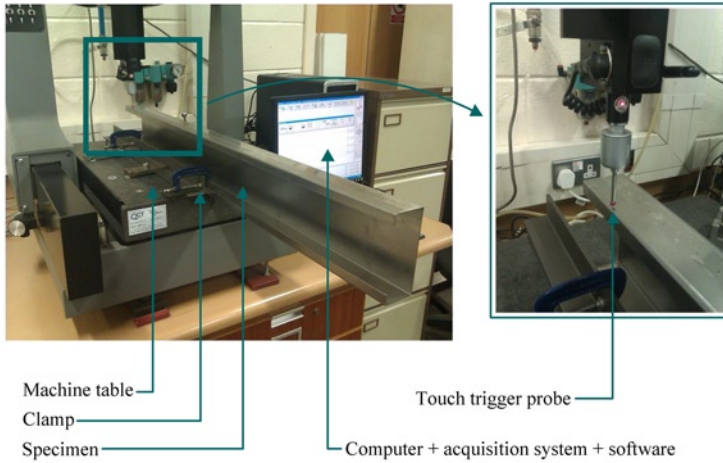
Fig. 6(b). Measuring geometric imperfections on the flange using the co-ordinate measuring machine.

5. Load-capacity upper-bound estimation via Yield Line Analysis (YLA)

5.1. YLA theoretical backgrounds

The yield line theory (Yield Line Analysis - YLA) applied to thin-walled steel structures enables an analysis of structural behaviour in the vicinity of ultimate load and in the post-ultimate stage. The basic assumption is that the plastic mechanism is fully developed, and the plastic zones developed in the walls of thin-walled steel members are concentrated at yield lines, either stationary or travelling [26, 27]. At the level of the yield lines, the material is considered to be fully plastic. Material characteristics is assumed to be rigid-perfectly plastic or rigid-plastic with strain hardening [15].

The theory distinguishes two types of the plastic mechanisms: a so-called "true mechanism" [26] and the so-called "quasi-mechanism", where the flat parts of the walls are limited by yield lines, but the walls undergo membrane deformation.

The plastic mechanism approach is based on two basic methods, namely the *energy method* (work method) and the *equilibrium strip method* [7, 16, 35]. In the present study only the energy method was applied. Using the energy method, the *Principle of Virtual Velocities* is adopted [14].

In the case of TWCFS members, the following form of this Principle, namely of the rate of change of the energy dissipated is usually applied:

$$\dot{\Pi}\left(\dot{\beta}, \chi\right) = \sum_i \int_{A_i} \left(N_0 \varepsilon_p\right) dA_i + \sum_j \dot{E}_{bi}\left(\dot{\beta} i, \bar{m}_{pi} \chi\right) \tag{1}$$

where Π is the potential energy of the system.

Eqn. (1) is a sum of rate of change of membrane strain energy in the walls of the global plastic hinge and bending strain energy dissipated at yield lines, where N_0 is a vector of membrane forces per unit length. The membrane forces N_0 are determined from the associated flow rule, considering corresponding yield criterion (e.g. Huber-Mises). A_i is an area of i-th plastic zone (tension field) vector, $\dot{\beta}_i$ is an angular velocity vector on the i-th yield line and $\bar{m}_{pi}$ is the plastic moment vector on that line.

The first component of Eqn. (1) is taken into account in the case of quasi-mechanisms only, which consist of both yield lines and plastic zones (tension fields). For the true mechanism only the second component of Eqn. (1) should be considered.

Rate of change of the energy dissipated at the rotation of two walls of the plastic mechanism along an i-th yield line is expressed as:

$$\dot{E}_{bi} = \int_0^{l_i} \bar{m}_{pi} \beta_i dl \tag{2}$$

For l_i = constant, the energy itself takes form:

$$E_{bi} = l_i \int_0^{\beta_i} \bar{m}_{pi} d\beta \tag{3}$$

where l_i is the length of the yield line and β_i is an angle of rotation along that line. The plastic moment in Eqn. (3) may be expressed by different equations, corresponding to different stress distributions assumed in the yield line cross-section [33]. For the fully plastic cross section, considering the rigid-perfectly plastic isotropic material model, the so called fully plastic moment takes the form [26]:

$$m_p = \frac{\sigma_y \cdot t^2}{4} \tag{4}$$

Thus, for the rigid-perfectly plastic material model, bending strain energy dissipated at i-th yield line is expressed as a product:

$$E_{bi} = l_i \cdot m_p \cdot \beta_i \tag{5}$$

After rearranging Eqn. (1) we obtain:

$$\delta W_{ext} = \delta E_b + \delta E_m \tag{6}$$

where δW_{ext} is the variation of work of external forces, δE_b is the variation of the energy of bending plastic deformation, while δE_m is the variation of the energy of membrane plastic deformation. Eqn. (6) provides a relation of generalised load (e.g. compressive load, bending moment) in terms of general displacement (e.g. shortening, the angle of rotation). The graphical representation of this relation will be termed in the present paper as a failure curve. Alternatively, Eqn. (6) may be rearranged into the following form:

$$P = \frac{\partial \left(E_b + E_m\right)}{\partial \delta} \tag{7}$$

5.2. Energy of Plastic Deformation in TWCFS Columns Subject to Compression Loading

In TWCFS columns subjected to compression the energy of plastic deformation is a sum of bending strain and membrane strain energy and generally may be expressed as follows:

$$E = E_b + \sum_{j=1}^k E_{mj} \tag{8}$$

where k is a number of tension fields.

The bending strain energy is given as follows:

$$E_b = m_p \sum_{i=1}^n l_i \cdot \beta_i \tag{9}$$

The membrane strain energy E_{mj} is the energy absorbed in tension fields, either in the web or in the flange (first component in Eqn. (1)):

$$E_{mj} = \int_{A_i} \left(N_0 \varepsilon_p \right) dA_i \qquad (10)$$

5.3. Theoretical Plastic Mechanism Model for Lipped-Channel Section Members with Perforations

Fig. 7. Comparison of experimental and FE deformation patterns in the post-ultimate state in the vicinity of the perforation with theoretical plastic mechanism model: (a) Set 1- perforations in the web (b) Set 2 – perforation in the flanges [22]

(c) – theoretical plastic mechanism model [34]
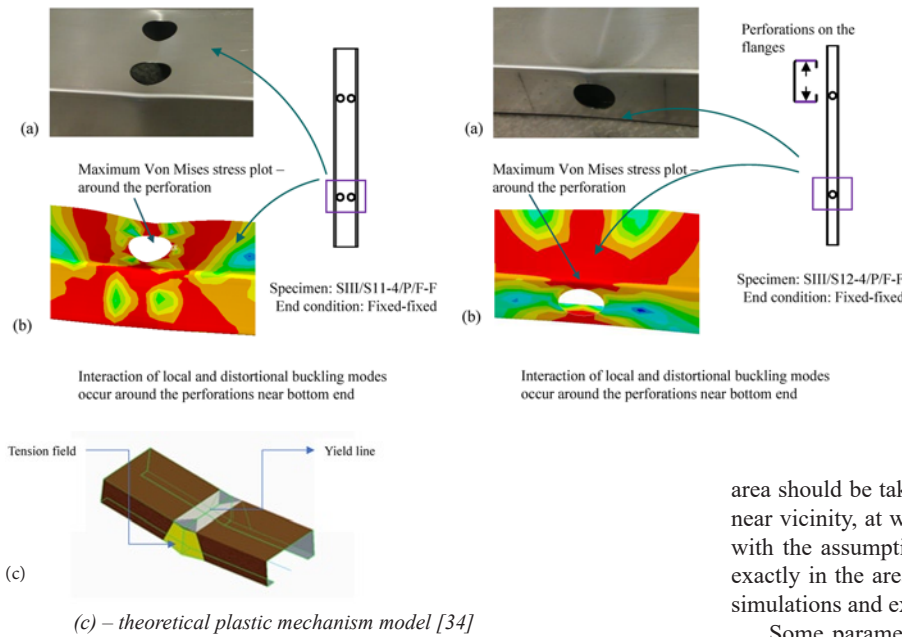
It was stated on the basis of experimental observations, that local plastic mechanisms were formed in all tested columns in the perforation area. The mechanism in both sets was of the same character, consisting of yield lines and tension

Fig. 8. Theoretical plastic mechanism model [34]; for better visibility of the figure tension fields □AGHB, □ICJD are not shadowed
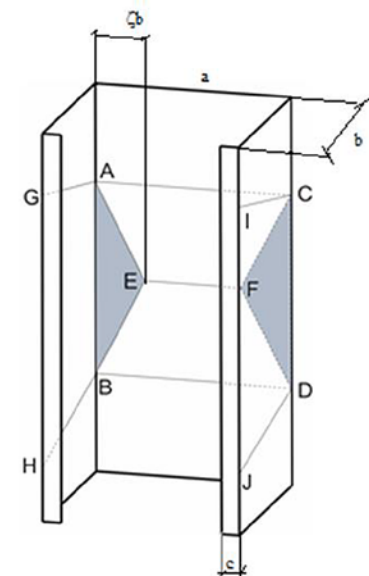
Table 6. Specification of yield lines and tension fields in the plastic mechanism model

Yield line/ tension field	Number of yield line/ tension field	Location
A C, BD	2	Web
A E, EB, …	4	Web
EF	1	Web
ΔAEB, ΔCFD	2	Web
A G, BH	4	Flange
□AGHB, □ICJD	2	flange

fields, both in the web and in the flanges, so that it was classified as quasi-mechanism [26]. (see Figure 7c). The theoretical model of this mechanism was derived (shown in Figure 9), based on failure modes, observed in experiments and obtained from FE simulations (Figure7a, b). Tension fields in the model are shadowed areas (dark grey and yellow in Fig. 7c). The similar mechanism model was originally derived for TWCFS lipped channel section columns subject to eccentric compression [3]. The mechanism is a combination of pitched-roof one in the web and so called CF true mechanism in the flanges, originally derived by Murray and Khoo and described in details in [27, 35]. The mechanism shown in Fig.7, after the modification and calibration due to the numerical and experimental results, was applied in YLA calculations in the present study. The geometry of the model is shown in Figure 9 and the specification of yield lines and tension fields is given in Table 6. Since in the analysis the rigid-perfectly plastic material model was assumed, the fully plastic moment (5) was taken into account. The wall thickness t was replaced by the equivalent thickness t* in relation (4):

$$m_p = \frac{\sigma_y \cdot (t^*)^2}{4} \qquad (11)$$

and in membrane energy of plastic deformation E_{mj}, given by (10), in tension fields.

The equivalent thickness was assumed to be reduced due to the perforation (t*=αt), where α is the reduction coefficient for perforated area. The reduction coefficient α was based on the ratio of the net width of a wall (b-b_p) to gross width b: $t^* = (1-b_p/b)t$. The weight of the net length of perforations along the member's axis (proposed by Davies [5]) was not taken into account, since in the case of YLA approach the net area should be taken for the very cross-section of perforation and its near vicinity, at which the plastic mechanism is formed. It coincides with the assumption, that the local plastic mechanism is developed exactly in the area of perforation, which was confirmed both by FE simulations and experimental tests.

Some parameters of the mechanism (among them ζ in Fig. 8 – [34]) should be determined (calibrated) on the basis of an experiment. The calibration of the mechanism model was performed for two sets of perforations separately. Within one set values of those parameters were the same. Detailed geometrical relations of this mechanism (particularly yield lines lengths l_i and rotation angles β_i in relation (4)), as well as membrane strain energy E_{mj} in tension fields (rel. 10) are given in [34].

5.4. Load-Carrying Capacity Upper-Bound Estimation Based on YLA

As mentioned above, upper-bound load- capacity estimation (l-c-c) is an intersection point of post-ultimate curve, obtained from (9) and post-buckling path. In the present solution, this point was obtained as an intersection of post-ultimate curve and extrapolated pre-buckling path. It is an allowable approximation, if a buckling load and ultimate load are close enough. The pre-buckling path of a column was derived, using the actual total compressive stiffness of the member with perforations. Exemplary load-
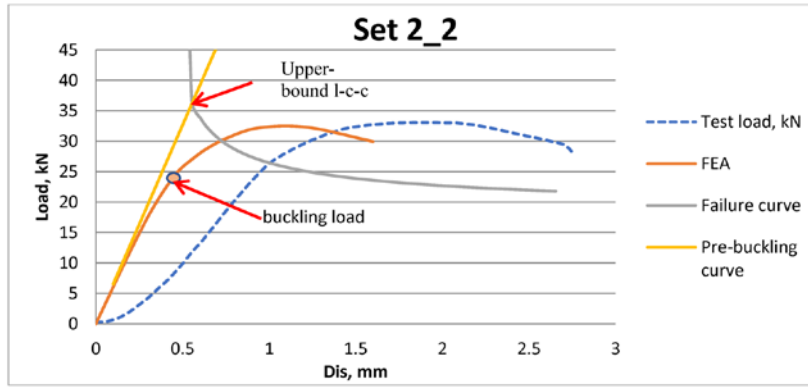
Fig. 9. Exemplary load-shortening diagra

6. Comparative analysis of numerical, theoretical and experimental result

The comparisons of numerical FE results, upper-bound l-c-c estimation results based on the analytical YLA approach and design code predictions computed from Eurocode [32] with experimental results are shown in Table 7 and 8. Since the European design code recommendations are based on ultimate load, only ultimate loads are compared. FE and test (experimental) values of ultimate loads are taken from the load-shortening diagrams, respectively.

Table 7. Ultimate strength (test results, numerical FE results, YLA results - upper-bound l-c-c, design code predictions) – Set 1

	Specimen	Ultimate Load (kN)				Ultimate Load Ratio			
		Test, $P_{exp, U}$	FEA $P_{FEA, U}$	YLA $P_{YLA, U}$	Eurocode, $N_{b,Rd}$	$P_{FEA, U}$ / $P_{exp, U}$	$P_{YLA,U}$ / $P_{exp, U}$	$N_{b,Rd}$ / $P_{exp, U}$	$N_{b,Rd}$/ $P_{YLA, U}$
Set 1	1-1	36.03	35.70	35.95	40.14	0.99	1.00	1.11	1.11
	1-2	35.42	38.52	34.55	39.04	1.09	0.98	1.10	1.13
	1-3	33.56	33.99	34.52	38.55	1.01	1.03	1.15	1.12
	1-4	33.40	32.63	34.49	38.65	0.98	1.03	1.16	1.12
	1-5	33.26	32.53	34.45	38.13	0.98	1.04	1.15	1.11
					Mean, $\bar{X}$	1.01	1.02	1.13	1.12
					Standard Deviation, S	0.05	0.03	0.95	0.01
					Coefficient of Variation, COV	0.05	0.02	0.02	0.01

Table 8. Ultimate strength (test results, numerical FE results, YLA results - upper-bound l-c-c, design code predictions) – Set 2

	Specimen	Ultimate Load (kN)				Ultimate Load Ratio			
		Test, $P_{exp, U}$	FEA $P_{FEA, U}$	YLA $P_{YLA, U}$	Eurocode, $N_{b,Rd}$	$P_{FEA, U}$ / $P_{exp, U}$	$P_{YLA,U}$ / $P_{exp, U}$	$N_{b,Rd}$ / $P_{exp, U}$	$N_{b,Rd}$/ $P_{YLA, U}$
Set 2	2-1	33.14	33.50	37.4	33.41	1.01	1.13	1.01	0.89
	2-2	33.05	32.30	36.56	31.46	0.98	1.11	0.95	0.85
	2-3	30.87	30.10	35.23	28.99	0.98	1.14	0.94	0.83
	2-4	29.78	28.60	34.49	27.48	0.96	1.16	0.92	0.80
	2-5	27.04	26.31	34.45	25.13	0.97	1.27	0.93	0.73
					Mean, $\bar{X}$	0.98	1.16	0.95	0.82
					Standard Deviation, S	0.02	0.06	0.04	0.06
					Coefficient of Variation, COV	0.02	0.05	0.04	0.07

shortening diagrams (analytical pre-buckling path and post-ultimate curve) together with FEA and experimental load-shortening diagrams are shown in Figure 10. The upper bound l-c-c estimation is indicated with the arrow. In the same way upper bound l-c-c was obtained for all columns under investigation. The results (ultimate loads) are shown in Table 7 and denoted as $P_{YLA, U}$.

7. Conclusions

The comparative analysis of numerical FE simulations, experimental and analytical load-capacity prediction based on YLA method, confirms the applicability of yield line approach to the upper-bound estimation of the load-carrying-capacity of TWCFS members with perforations subject to axial compression.

This approach is competitive with FE simulations due to the simplicity of algorithms. It also may be used to perform an advanced structural analysis based on performance criteria [35].
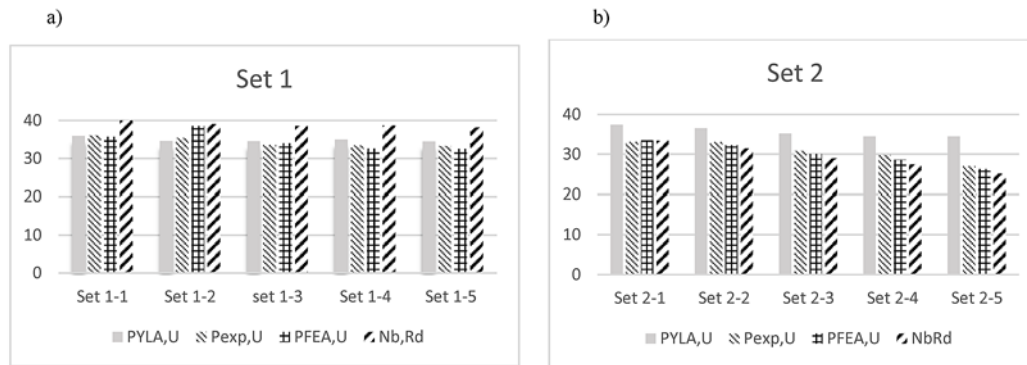
Fig. 10. Comparison of ultimate load predictions: a) set 1 – perforations in the web, b) – set 2- perforations in the flanges

The agreement of ultimate loads obtained as upper-bound estimation via YLA approach with FE and experimental results is very good for members with perforations on the web (Set 1). In that case code predictions overestimate theoretical and experimental results.

For members with perforations on the flanges the agreement of upper-bound load-carrying capacity via YLA with experimental and FE results is worse (maximum discrepancy about 25%). In that case more accurate calibration and modification of plastic mechanism model is necessary. Code predictions for that case slightly underestimate experimental and FE results and significantly underestimate load-carrying capacity via YLA approach. However, the latter is related also to the overestimation of load-capacity using the YLA method in comparison with experiment and FE simulations.

The obtained comparative results also indicated that current design rules in the European Recommendations predict not exactly the load capacity of TWCFS lipped channel column members with perforations subjected to axial compression loading and require further investigation through more extensive testing of a wider range of structural cross-sections.

References

1. ANSYS ANSYS Mechanical APDL Structural Analysis Guide: ANSYS Release 13.0. - 2010.
2. Brockenbrough R. L. Highway Engineering Handbook. McGraw-Hill Education, 2009. - ISBN: 9780071597630LCCN: 2009002381.
3. Cardoso F. System reliability-based criteria for the design of steel storage rack framesby advanced analysis: Part II - Reliability analysis and design applications. Thin-Walled Structures 2019; 141: 725-739, https://doi.org/10.1016/j.tws.2019.03.021.
4. Camotim D. Local post-buckling behavior of cold-formed steel rack columns. Proceedings. of 3th CIMS Conference (CIMS2000), Lisbon, Imperial College Press 2000: 213-222, https://doi.org/10.1142/9781848160095_0025.
5. Davies M. The design ofperforated cold-formed steel sections subject to axial load and bending. Thin-Walled Structures 1997; 29/1-4: 141-157, https://doi.org/10.1016/S0263-8231(97)00024-4.
6. Falkowicz K. Numerical analysis of compressed plates with a cut-out operating in the geometrically non-linear range. Eksploatacja i Niezawodnosc - Maintenace and Reliability 2015; 17 (2): 222-227, https://doi.org/10.17531/ein.2015.2.8.
7. Flockhart CJ, Murray NW, Grzebieta R H. Comparison of upper-bound rigid-plastic yield line mechanism analysis by the energy and equilibrium strip method. Proc. of the 2nd Australasia Congress of Applied Mechanics. Canberra, 1999.
8. Grenda M, Paczos P. Experimental and numerical study of local stability of non-standard thin-walled channel beams. Journal of Theoretical and Applied Mechanics 2019; 57: 549-562, https://doi.org/10.15632/jtam-pl/109601.
9. Hutton DV. Fundamentals of Finite Element Analysis - McGraw-Hill, 2004. - ISBN: 9780072395365LCCN: 2003048735.
10. Institution British Standards BS5950 1998: British Standards for Structural Use of Steel Work in Buildings. Part 5: Code of Practice for Design of Cold Formed Thin Gauge Sections. 1998.
11. Iron American i Institute Steel North American Specification for the Design of Cold-formed Steel Structural Members. American Iron and Steel Institute, 2016.
12. Kolakowski Z. A semi-analytical method for the analysis of the interactive buckling of thin-walled elastic structures in the second order approximation., Int. J. Solids Structures 1996; 33(25): 3779-3090, https://doi.org/10.1016/0020-7683(95)00211-1.
13. Kotełko M, Lis P, Macdonald M. Load-Capacity Probabilistic Sensitivity Analysis of Thin-Walled Beams. Proceedings of the 7th International Conference on Thin Walled Structures. Busan. 2014.
14. Kotełko M. Load-capacity and mechanisms of failure of thin-walled structures (in Polish - Nośność i mechanizmy zniszczenia konstrukcji cienkościennych), Wydawnictwa Naukowo-Techniczne, 2011.
15. Kotełko M. Load-capacity estimation and collapse analysis of thin-walled beams and columns-recent advances. Thin-Walled Structures 2004; 42: 153-175, https://doi.org/10.1016/S0263-8231(03)00055-7.
16. Kotełko M, Mania R. Alternative solutions of the problem of load-capacity of thin-walled plated structures. Mechanics and Mechanical Engineering. 2008; 2: 323-336.
17. Kulatunga M P. Load capacity of cold-formed column members of lipped channel cross-section with perforations subjected to compression loading - Part I: FE simulation and test results. Thin-Walled Structures 2014; 80: 1-12, https://doi.org/10.1016/j.tws.2014.02.017.
18. Kulatunga M, Macdonald M. Investigation of cold-formed steel structural members with perforations of different arrangements subjected to compression loading. Thin-Walled Structures 2013; 67: 78-87, https://doi.org/10.1016/j.tws.2013.02.014.
19. Kulatunga M, Macdonald M. Investigation of Cold-Formed Steel Structural Members With Perforations of Different Shapes Subjected to Compression Loading. Proceedings of the 6th International Conference on Couple Instabilities in Metal Structures. Busan 2012, https://doi.org/10.1016/j.tws.2013.02.014.

20. Kulatunga M, Macdonald M. The Efficient Design of Cold-Formed Perforated Thin-Walled Steel Structural Member Subjected to Compression Loading. Proceedings of the 7th International Conference on Thin Walled Structures. Glasgow 2014.
21. Liew JYR, Thevendran V, Shanmugam NE. Thin-Walled Structures: Research and Development. Elsevier Science, 1998.
22. Macdonald M, Kulatunga M, Kotełko M. The effects of compression loading on perforated cold-formed thin-walled steel structural members of lipped-channel cross-section. AIP Conference Proceedings 2019, https://doi.org/10.1063/1.5086138.
23. Magnucka-Blandzi E. Effective shaping of cold-formed thin-walled channel beams with double-box flanges in pure bending. Thin-Walled Structures 2011; 49: 121-128, https://doi.org/10.1016/j.tws.2010.08.013.
24. Moen C, Schafer B. Direct Strength Method for Design of Cold-Formed Steel Columns with Holes. Journal of Structural Engineering-ASCE 2010; 137, https://doi.org/10.1061/(ASCE)ST.1943-541X.0000310.
25. Moen C, Schafer B. Experiments on cold-formed steel columns with holes. Thin-walled Structures - Thin Wall Structures 2008; 46: 1164-1182, https://doi.org/10.1016/j.tws.2008.01.021.
26. Murray N W. Introduction to the Theory of Thin-Walled Structures. Clarendon Press, 1986.
27. Murray N W, Khoo P. S. Some basic plastic mechanisms in the local buckling of thin-walled steel structures. International Journal of Mechanical Sciences 1981; 23: 703-713, https://doi.org/10.1016/0020-7403(81)90008-4.
28. Nedelcu M. Buckling mode identification of perforated thin-walled members by using GBT and shell FEA. Thin-Walled Structures 2014, 82: 67-81, https://doi.org/10.1016/j.tws.2014.04.005.
29. Rhodes J. Design Cold Form Steel Members. Taylor & Francis, 1991.
30. Schafer B. Review: The Direct Strength Method of cold-formed steel member design. Journal of Constructional Steel Research 2008; 64 (7-8): 766-778, https://doi.org/10.1016/j.jcsr.2008.01.022.
31. Schafer B, Peköz T. Computational modeling of cold-formed steel: Characterizing geometric imperfections and residual stresses. Journal of Constructional Steel Research 1998; 47: 193-210, https://doi.org/10.1016/S0143-974X(98)00007-8.
32. Standardization European Committee EN 1993-1-3:2006, Eurocode 3., 2009, Design of Steel Structures; Part 1.3: General Rules - Supplementary Rules for Cold Formed Thin Gauge Members and Sheeting. - Brussels : CEN, 2009.
33. Teter A, Kołakowski Z. Lower bound estimation of load-carrying capacity of thin-walled structures with intermediate stiffeners. Thin-Walled Structures 2001; 39(8): 649-669, https://doi.org/10.1016/S0263-8231(01)00028-3.
34. Ungureanu V. et all. Plastic mechanisms of thin-walled cold-formed steel members in eccentric compression. Thin-Walled Structures 2018; 63: 183-206, https://doi.org/10.1063/1.5019077.
35. Ungureanu V, Kotełko M, Dubina D. Ultimate limit capacity of thin-walled cold-formed steel members. Ro. J. Techn. Sci. Appl. Mechanics 2018; 128: 184-192, https://doi.org/10.1016/j.tws.2017.09.029.
36. Xiao-Ling Z. Yield line mechanism analysis of steel members and connections. Progress in Structural Engineering and Materials 2003; 5: 252-262, https://doi.org/10.1002/pse.161.
37. Yan Qi L. Analysis and design reliability of axially compressed members with high-strength cold-formed thin-walled steel. Thin-Walled Structures 2007; 45: 473-492, https://doi.org/10.1016/j.tws.2007.02.012.
38. Yao Z, Rasmussen K. Inelastic local buckling behaviour of perforated plates and sections under compression. Thin-Walled Structures 2012; 61: 49-70, https://doi.org/10.1016/j.tws.2012.07.002.
39. Yu W. W. Cold-Formed Steel Design. Wiley, 2000.

Maria KOTELKO
Department of Strength of Materials
Lodz University of Technology
ul. Stefanowskiego, 90-924 Lodz, Poland

Martin MACDONALD
Muditha P. KULATUNGA
Department of Mechanical Engineering,
School of Computing, Engineering & Built Environment
Glasgow Caledonian University
Cowcaddens Rd, Glasgow G4 0BA, UK

Zuzanna MARSZALEK
Department of Strength of Materials
Lodz University of Technology
ul. Stefanowskiego, 90-924 Lodz, Poland

E-mails: maria.kotelko@p.lodz.pl, M.Macdonald@gcu.ac.uk,
muditha.kulatunga@gcu.ac.uk, jaros.zuzanna@gmail.com